quantum beam science

MDPI

Article

Microstructural Analysis, Compressive Strength, and Wear Properties of Spark-Plasma-Sintered Al–Mg–PPA Composites

Osarue Osaruene Edosa [1], Francis Kunzi Tekweme [1], Peter A. Olubambi [2] and Kapil Gupta [1,*]

[1] Department of Mechanical and Industrial Engineering Technology, University of Johannesburg, Johannesburg 2028, South Africa; oedosa@uj.ac.za (O.O.E.); ftekweme@uj.ac.za (F.K.T.)
[2] Centre for Nanoengineering and Advanced Materials, School of Mining, Metallurgy and Chemical Engineering, University of Johannesburg, Johannesburg 2028, South Africa; polubambi@uj.ac.za
* Correspondence: kgupta@uj.ac.za

Abstract: One technique for sintering green compacts and imparting the required qualities to meet the specific application requirements is spark plasma sintering (SPS). This study examines the effects of SPS parameters (sintering temperature and pressure, holding time, and heating rate) and plantain peel ash (PPA) reinforcement concentrations (0, 5 wt%, 10 wt%, 15 wt%, and 20 wt%) on the microstructure, compressive strength, and wear characteristics of the fabricated Al–Mg–PPA composites. As a result of the ball milling machine's high efficiency, the PPA reinforcement was evenly dispersed throughout the aluminum matrix after 90 min of milling. At lower sintering temperatures and pressures, microstructural flaws such as weak grain boundaries, micro-pores, and micro-cracks were more noticeable than at higher ones. The PPA reinforcement and magnesium powder (wetting agent) increased the composites' compressive strength by improving the wettability between the PPA reinforcement and the Al matrix. At a weight fraction of 5 wt% PPA, the maximum compressive strength of 432 MPa was attained for the sintered composites, which is a 222% improvement over the sintered aluminum matrix. Additionally, the PPA reinforcement enhanced the wear properties of the sintered Al–Mg–PPA composites by reducing the wear loss. Increasing the wear load resulted in a higher wear rate. The COF for the sintered composites ranges from 0.049 to 0.727. The most consistent correlation between the wear rate and the COF is that as the wear rate decreases, the COF decreases, and vice versa. Abrasive wear was the dominant wear mechanism observed. Tear ridges, shear steps, micro-voids, and cleavages were seen on the composites' fracture surfaces, an indication of a ductile-brittle fracture.

Keywords: Al matrix composites; compressive strength; wear; microstructure; plantain peel ash; spark plasma sintering

check for updates

Citation: Edosa, O.O.; Tekweme, F.K.; Olubambi, P.A.; Gupta, K. Microstructural Analysis, Compressive Strength, and Wear Properties of Spark-Plasma-Sintered Al–Mg–PPA Composites. *Quantum Beam Sci.* **2024**, *8*, 32. https://doi.org/10.3390/qubs8040032

Academic Editor: Swee Leong Sing

Received: 31 October 2024
Revised: 4 December 2024
Accepted: 12 December 2024
Published: 17 December 2024

Copyright: © 2024 by the authors. Licensee MDPI, Basel, Switzerland. This article is an open access article distributed under the terms and conditions of the Creative Commons Attribution (CC BY) license (https://creativecommons.org/licenses/by/4.0/).

1. Introduction

The increasing demand for aluminum matrix composites (AMCs) drives additional research aimed at enhancing their properties. Currently, industries require materials that can outperform expectations regarding quality and functionality when employed in manufacturing. Such materials are anticipated to possess a wide range of properties, including high stiffness, strength-to-weight ratio, high modulus, ductility, high corrosion resistance, high machinability, and weldability, which may not be achievable with monolithic materials [1,2]. Reinforcement materials play a major role in the application and performance of AMCs. By enhancing their properties, the reinforcement material provides the composites additional support. They also alter the properties of the composites for more extensive applications. Additionally, the properties of AMCs can be influenced by the type of reinforcements, the volume fraction, and the particles' size and shape [3]. Al_2O_3, fly ash, TiB_2, SiC, TiC, RHA, B_4C, Gr, carbon nanotubes (CNTs), fullerene, and graphene are common reinforcements for fabricating AMCs. The purpose of these reinforcements is to achieve tailored properties. For

instance, CNT, fullerene, and graphene offer unique self-lubricating properties to AMCs, enhancing their wear-resistant properties [4–6]. Other reinforcements like TiC, fly ash, B_4C, and SiC increased the wear resistance of AMCs by enhancing the hardness property [7,8]. Some of the areas of applications of AMCs include engine pistons, brake parts, extruded channels and angles, and electronic packaging [4,9,10]. AMCs are reportedly well-suited for automobile brake applications due to their unique characteristics [11–13]. Aluminum alloys and their composites are easily oxidized to form a thin film of oxide layer that limits material flow and lowers wear rate. The thin film of the oxide layer acts as a lubricant that protects against wear [14].

Furthermore, the manufacturing process is another factor that can influence the quality of AMCs. The efficacy of the processing technique, reinforcement geometry, and cost are some factors that can influence the choice of production method. Several methods have been employed for fabricating AMCs. As reported, the production routes for AMCs include solid state, liquid state, liquid–vapor state, and in situ. Examples include stir-casting, squeeze-casting, powder metallurgy, and friction stir processes [15–17].

The suitability of the SPS technology in producing high-quality AMCs is examined in this study. High-energy ball milling and SPS processing were used to fabricate the composite samples in this research. Reducing porosity and enhancing microstructural features have been the ultimate goals of every processing technology. The SPS process is a variant of the conventional powder metallurgy, which does not require a separate compaction stage. Compaction and sintering of compacts are performed simultaneously. The SPS process is a pressure-assisted process that uses a pulsed current to generate a large amount of heat needed for rapid powder consolidation. Its advantages over other fabrication processes, such as stir-casting and squeeze casting, include improved microstructural features such as grain boundaries, grain distribution, and orientation with little to no defects; improved mechanical properties such as strength, ductility, and hardness; little to no undesirable interfacial reaction/precipitation; and suitability for various engineering materials such as super-alloys, composites, metallic glasses, metals, and ceramics [18].

The essential steps in the spark plasma sintering process include removing gas to create a vacuum atmosphere, compaction pressure to transmute the loose powder into a solid mass, heating and holding to further consolidate the solid mass, and cooling to room temperature. Higher heating rates and lower compaction pressures are two benefits of the SPS process over the traditional powder metallurgy process. An SPS machine can heat up to 1000 °C/min compared to a conventional sintering machine. Thus, it takes less time to reach the desired sintering temperature, less time to hold the grain in place, and a higher diffusion rate to create a stronger and cleaner interfacial bond [1,19]. Similarly, excessive compaction pressure may result in particle/fiber damage, raising porosity [20]. This study develops aluminum matrix composites using pure aluminum powder as the matrix, plantain peel ash (PPA) as the reinforcement, and pure magnesium powder as the wetting agent in a unique combination (Al–Mg–PPA) never reported in the literature. It also examines the effects of SPS parameters and PPA reinforcement concentration on the sintered Al–Mg–PPA composites' microstructure, compressive strength, and wear resistance.

2. Materials and Method

2.1. Design and Production of Al–Mg–PPA Composites

The starting materials for this study are pure aluminum powder (purity > 99%, average particle size 75 μm, obtained from Zimco Aluminum Company, Benoni, South Africa), which was used as the metal matrix; plantain peel ash (average particle size 70 μm, obtained from Harper, Maryland County, Republic of Liberia) used as the reinforcement; and pure magnesium powder (purity > 99%, average particle size 100 μm, obtained from Sigma-Aldrich, South Africa) used as the wetting agent. Percentage weight fractions of 0, 5, 10, 15, and 20 wt% PPA were used to reinforce the aluminum matrix. A fixed 2 wt% Mg was added to the composite powder mixtures as a wetting agent. Tables 1 and 2 show the

chemical compositions of the pure aluminum and PPA reinforcement, respectively. The design of experiments was performed using the Taguchi method. An orthogonal array (OA) of ($L_{25}5^5$) was used to organize the control parameters at different levels.

Table 1. Elemental percentage composition of pure aluminum powder.

Cu	Mg	Si	Fe	Mn	Ni	Zn	Ti	Pb	Sn	Al
0.02	0.01	0.2	0.31	0.01	0.01	0.02	0.01	0.01	0.01	99.30

Table 2. Chemical composition of PPA.

SiO_2	Al_2O_3	MgO	K_2O	Fe_2O_3	P_2O_5	Others
4.18	1.45	1.26	79.42	4.70	4.46	Balance

The Al–Mg–PPA composite samples were synthesized using a ball milling machine (PM 100, Retsch, Haan, Germany) and an SPS machine (8604 HHPD25) with a working temperature of 2200 °C and a maximum pressing force of 250 KN. The powder mixing parameters include a ball-to-powder weight ratio (BPR) of 5:1, a milling time of 90 min, an average milling speed of 200 rpm, and 1 wt% propanol as a process control agent (PCA). The milling machine uses a vacuum atmosphere to prevent powder contamination or oxidation and stops for 10 min every 30 min of operation to prevent a temperature rise in the milling vial. The powder mixtures were charged into a 20 mm graphite die for compaction and sintering following milling. Each composite sample produced has an average diameter of 20 mm and a height of 12 mm. The processing parameters are presented in Table 3. Figure 1 presents the processing sequence and equipment for fabricating, characterizing, and testing the Al–Mg–PPA composite samples. A minimum of twenty-five samples were produced due to the ($L_{25}5^5$) orthogonal array. The sintered samples were numbered accordingly for easy identification.

Table 3. Input parameters and levels for ($L_{25}5^5$) orthogonal array.

Input Parameters	Levels				
	1	2	3	4	5
Sintering temperature (°C)	430	460	490	520	550
Holding time (min)	2	4	6	8	10
Sintering pressure (MPa)	12	22	32	42	52
Heating rate (°C/min)	50	100	150	200	250
Reinforcement (wt%)	20	15	10	5	0

2.2. Compression Test

The compression test for the Al/Mg/PPA composite samples was conducted according to ASTM E9–19 standards using an Instron universal testing machine 6800 series with a maximum load capacity of 300 KN, equipped with suitable compression platens, a deflectometer, and software capable of strain rate control. Before the compression test, the sample gauge sections' diameter, height, and cross-sectional area were measured using a caliper. Each specimen for the test has a semi-cylindrical shape with a diameter of 20 mm and a height of 12 mm. The test was conducted at room temperature and pressure. The composites' ultimate engineering compressive strength (σ_{uc}) was determined using the ratio of maximum compressive force to initial cross-sectional area.

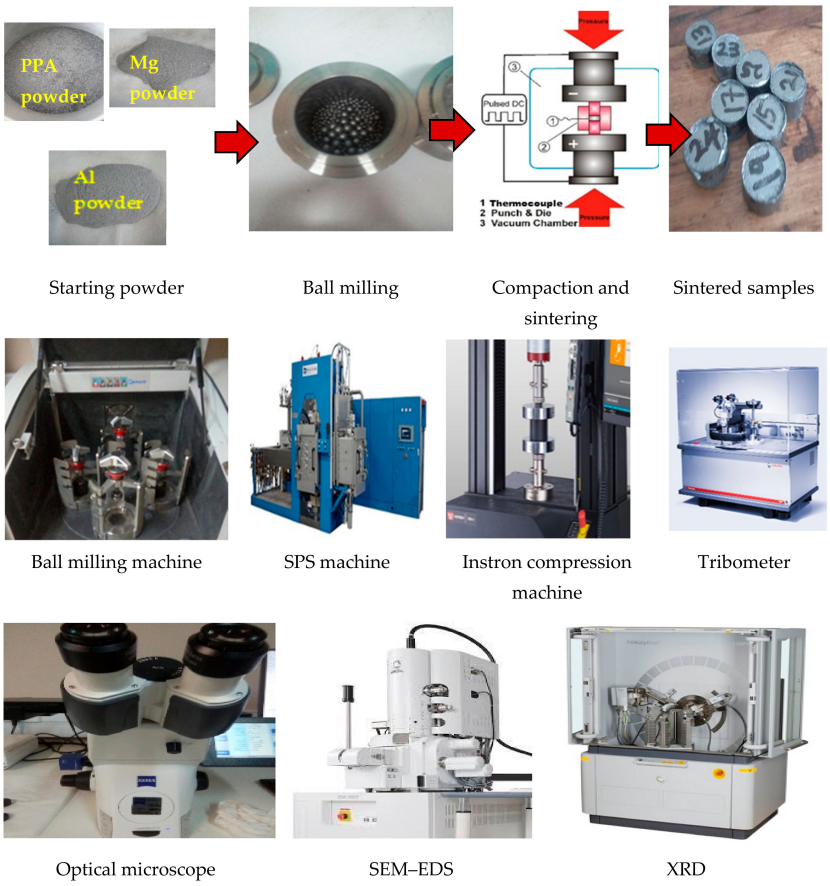


Figure 1. Processing sequence and equipment for fabricating, characterizing, and testing of ($L_{25}5^5$) Al/Mg/PPA composites.

2.3. Wear Test

The wear test for the newly developed Al/Mg/PPA composite samples is essential to determine the tribological properties of the material. This study used a TRB pin-on-disc tribometer (Anton Paar) for the wear test following ASTM G99 standards under dry sliding conditions. Before the test, the samples were prepared in semi-cylindrical shapes with a diameter of 20 mm and a height of 12 mm. Parameters for the wear test include applied loads of 2 N and 5 N, sliding distance of 5 m, and a velocity of 1 cm/s. The mass loss, a determinant of wearing, was obtained by finding the difference between the initial and final mass of the composite samples. The volume loss, wear rate, and wear resistance can be evaluated using Equation (1)–(3), respectively [21].

$$volume\ loss = \frac{mass\ loss}{density} \times 1000 \tag{1}$$

$$wear\ rate = \frac{Volume\ loss}{Applied\ load \times sliding\ distance} \tag{2}$$

$$wear\ resistance = \frac{applied\ load \times sliding\ distance}{volume\ loss} \tag{3}$$

2.4. Microstructural Characterization

The sintered Al–Mg–PPA composite samples were cut laterally into the desired sizes using a precision cutting machine (ATM Brillant 220) and prepared following the standard metallographic procedure before microstructural examinations. Etching was performed using Keller reagent (95 mL distilled water + 2.5 mL HNO3 + 1.5 mL HCl + 1.0 mL HF). The

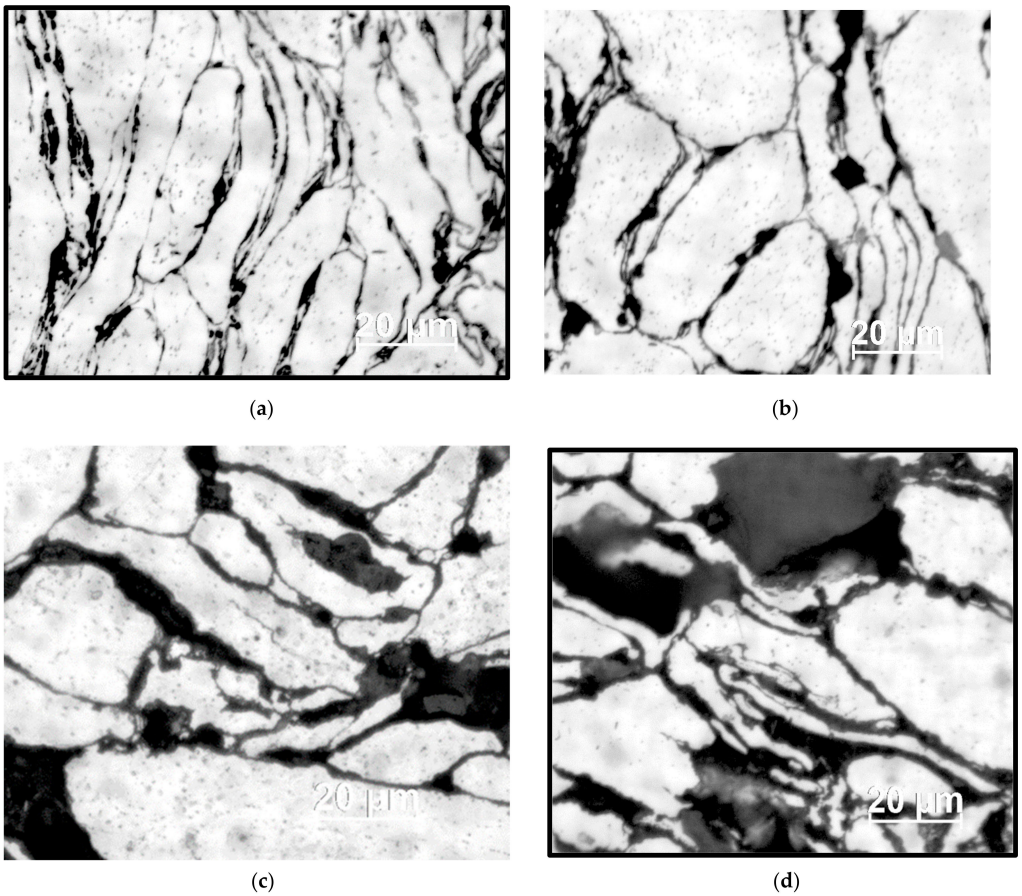
surface morphology of the composites was examined using an optical microscope (ZEISS model), the microstructural features were analyzed using SEM (JEOL 7900F) equipped with energy-dispersive spectroscopy (EDS), and the composites' phases were analyzed using an X-ray diffractometer.

3. Results and Discussion

3.1. Microstructural Analysis

3.1.1. Optical Microscopy

The optical micrographs of the sintered Al–Mg–PPA composites are presented in Figure 2a–d. It can be seen from Figure 2 that the PPA and Mg particles are well dispersed over the Al matrix, confirming that the ball milling process is an efficient powder mixing method. The composites' powder particles' homogeneity is required for improved mechanical properties [22]. Oval, irregular, and flaky grain shapes, mixed grain size distribution, few grain clusters, and tiny pores characterize the composites' microstructures. The grain size distribution, which ranges from 20 µm to 140 µm in the microstructures of the sintered Al–Mg–PPA composites shown in Figures 2 and 3, using Image J software, confirms the fracturing of some of the coarse particles into fine grains. The variation in the particle sizes of the microstructures is a great advantage because mixed grain sizes are more misaligned, leading to better particle packing. This enhances grain boundaries and mechanical properties.



(**a**) (**b**)

(**c**) (**d**)

Figure 2. Optical micrographs of AMCs (**a**) Al–2Mg, (**b**) Al–2Mg–5PPA, (**c**) Al–2Mg–15PPA, and (**d**) Al–2Mg–20PPA.

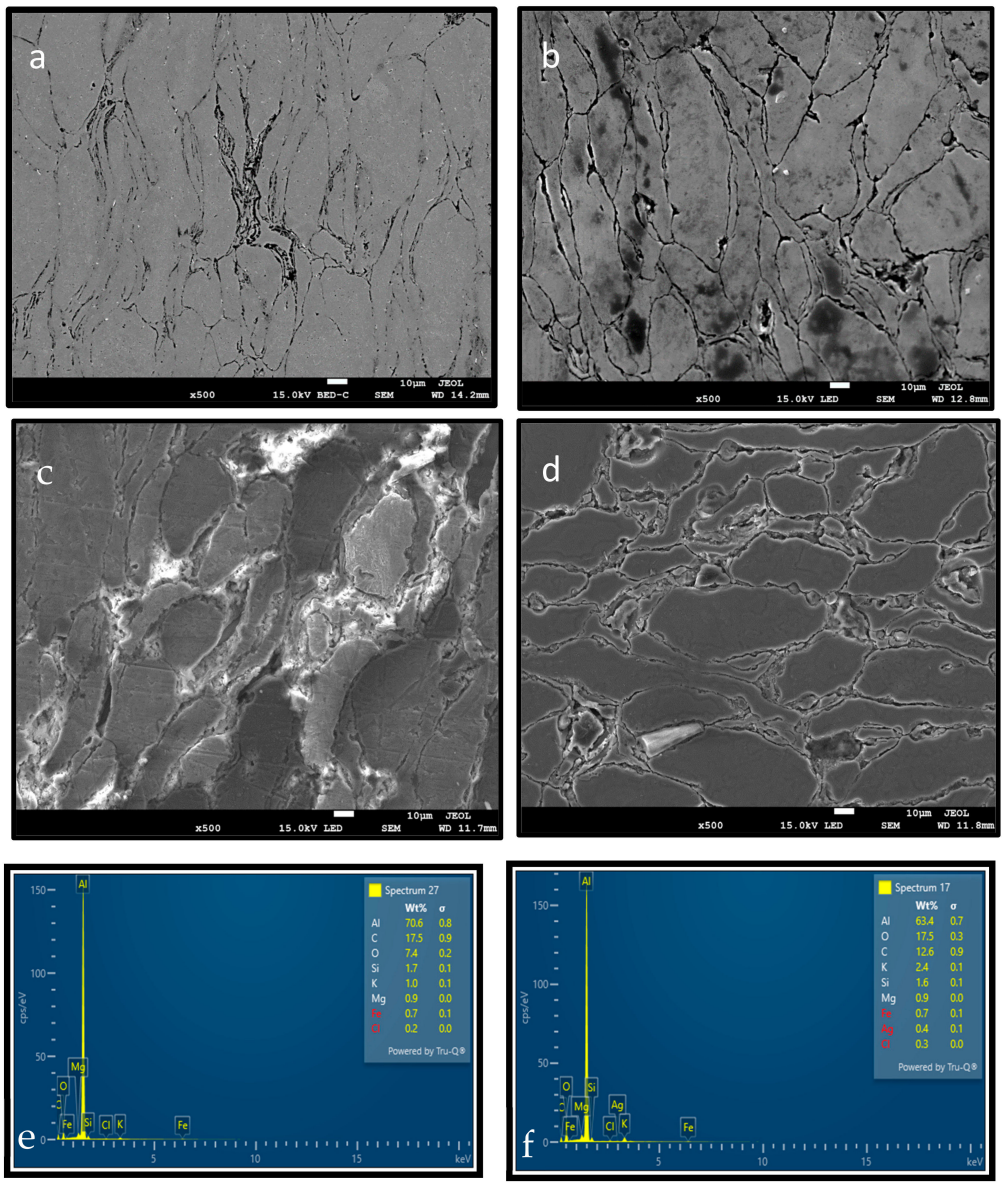


Figure 3. SEM micrographs of AMCs (**a**) Al–2Mg, (**b**) Al–2Mg–5PPA, (**c**) Al–2Mg–20PPA@430 °C, (**d**) Al–2Mg–20PPA@550 °C; (**e**) Al–2Mg–5PPA—EDS and (**f**) Al–2Mg–20PPA—EDS.

3.1.2. SEM–EDS

The SEM micrographs and EDS analysis of the sintered Al–Mg–PPA composite samples are presented in Figure 3a–f. The processing parameters for the samples in Figure 3 are (3a) Al–2Mg (ST = 550 °C, SP = 32 MPa, HT = 4 min, and HR = 200 °C/min), (3b) Al–2Mg–5PPA (ST = 490 °C, SP = 22 MPa, HT = 10 min, and HR = 50 °C/min), (3c) Al–2Mg–20PPA (ST = 430 °C, SP = 12 MPa, HT = 2 min, and HR = 50 °C/min), and (3d) Al–2Mg–20PPA (ST = 550 °C, SP = 22 MPa, HT = 6 min, and HR = 250 °C/min). It is obvious from the Figure that apart from Figure 3c, the grains of the composites are well aligned with no significant agglomeration. Comparing the microstructure of Figure 3a (not reinforced with PPA reinforcement) with the microstructures of Figure 3b–d reinforced with PPA reveals that adding PPA to the Al matrix and sintering at elevated temperatures improves the composite's microstructural features such as grain boundaries by promoting better particle packing and alignment and reducing pores. More so, for stronger consolidation of AMC, high thermal energy is required. This explains why the microstructure in Figure 3c sintered at 430 °C exhibited poor grain boundaries and other microstructural defects compared with Figure 3b sintered at 550 °C, despite having the same composition (Al–2Mg–20PPA). Additionally, it is obvious that interfa-

cial precipitations are distributed in the grain boundaries. These precipitations are more with composites reinforced with high-volume PPA. As indicated by the EDS analysis shown in Figure 3e,f, the PPA contains a considerable percentage weight fraction of carbon (C). During sintering at elevated temperatures, carbide precipitations, such as expressed in Equation (4), become unavoidable [19,23]. High-volume Al_4C_3 can increase brittleness in AMC.

$$4Al + 3C = Al_4C_3 \quad (4)$$

3.1.3. X-Ray Diffractometer

The XRD patterns for the sintered Al–Mg–PPA composites are shown in Figure 4. The intensity of the diffraction peaks indicates the presence of major and minor phases. The material phases before milling and sintering are aluminum, magnesium, and plantain peel ash (K_2O, SiO_2, Fe_2O_3, and P_2O_5).

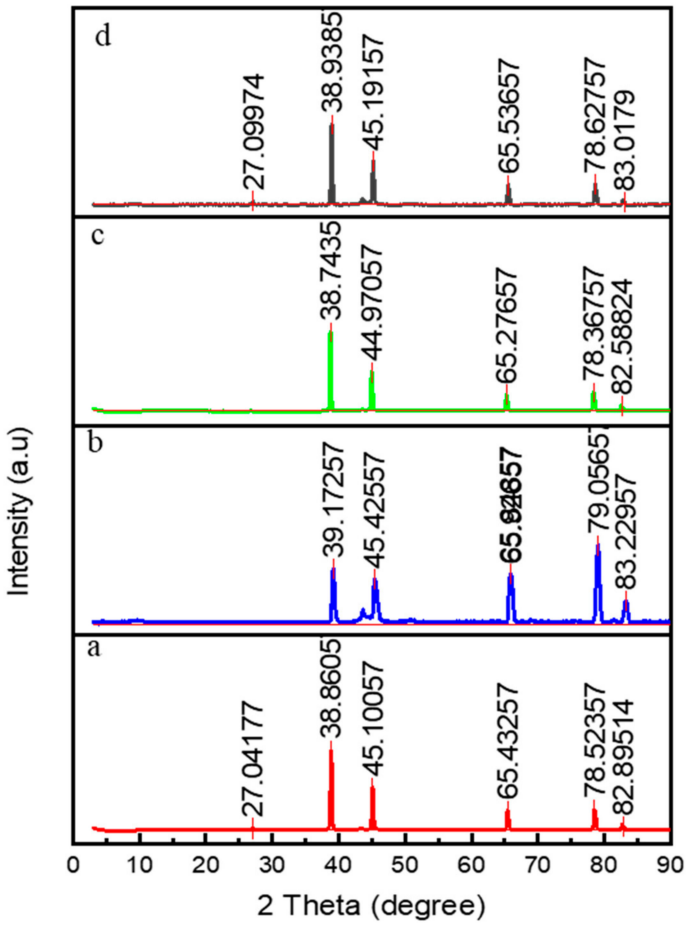


Figure 4. XRD patterns for Al–Mg–PPA samples (**a**) Al–2Mg–15PPA, (**b**) Al–2Mg–20PPA@520 °C, (**c**) Al–2Mg, and (**d**) Al–2Mg–20PPA@550 °C.

From Figure 4, the major phases correspond to peaks with the highest intensities. As reported, intermetallic phases such as Al_3Mg_2 and $Al_{12}Mg_{17}$ develop when the aluminum matrix is reinforced with magnesium [1]. Using X'Pert HighScore 5.2 software and from the literature, it was discovered that the Al phase corresponds to peak angles of 38.7, 38.8, 38.9, 65.2, and 83.2; the Mg phase corresponds to 44.9 and 81.5; the $Al_{12}Mg_{17}$ phase corresponds to 82.59; the Al_2O_3 phase corresponds to 39.17 and 45.4; the MgO phase corresponds to 78.6; and the $MgAl_2O_4$ phase corresponds to 45.1°. The aluminum oxide phase acts as a lubricant and protective layer, which improves wear resistance. The Al–Mg phase may also be responsible for the improved interfacial bond strength and mechanical properties.

3.2. Taguchi Analysis

The Taguchi analysis for compressive strength and wear resistance aims to maximize the strength and minimize the wear rate of the sintered Al–Mg–PPA composites. With the aid of Minitab 20 software, both the larger-the-better (compressive strength) and the smaller-the-better (wear rate) approaches have been used, as expressed in Equations (5) and (6) as follows:

$$SN_L = -10\log\left(\frac{1}{n}\sum_{i=1}^{n}\frac{1}{y_i^2}\right) \quad (5)$$

$$SN_S = -10\log\left(\frac{1}{n}\sum_{i=1}^{n}y_i^2\right) \quad (6)$$

where y_i is the experimental result (response) and n is the number of trials for y_i.

3.3. Compressive Strength

The engineering stress–strain curves of the sintered Al–Mg–PPA samples having distinct elastic and plastic regions are illustrated in Figure 5. As presented in Table 4, the sintering parameters for the samples in Figure 5 are Al (ST = 550, SP = 12 MPa, HT = 4 min, and HR = 200 °C/min), Al–2Mg (ST = 430, SP = 52 MPa, HT = 10 min, and HR = 250 °C/min), Al–2Mg–5PPA (ST = 460, SP = 32 MPa, HT = 4 min, and HR = 250 °C/min), Al–2Mg–10PPA (ST = 460, SP = 22 MPa, HT = 2 min, and HR = 200 °C/min), Al–2Mg–15PPA (ST = 460 °C, SP = 12 MPa, HT = 10 min, and HR = 150 °C/min), and Al–2Mg–20PPA (ST = 490, SP = 42 MPa, HT = 4 min, and HR = 150 °C/min). The figure makes it clear that the Al–Mg–PPA samples' compressive strengths are higher than that of the sintered aluminum matrix, with composite samples displaying reduced compressive strength as the PPA reinforcement concentration increases. Figure 6 indicates that 5 wt% PPA is the optimal reinforcement weight fraction for the sintered composite samples. Factors such as the matrix-reinforcement characteristics, interfacial bonding strength, and sintering parameters such as the sintering temperature and pressure, holding time, and heating rate may have influenced the compressive strength [24,25].

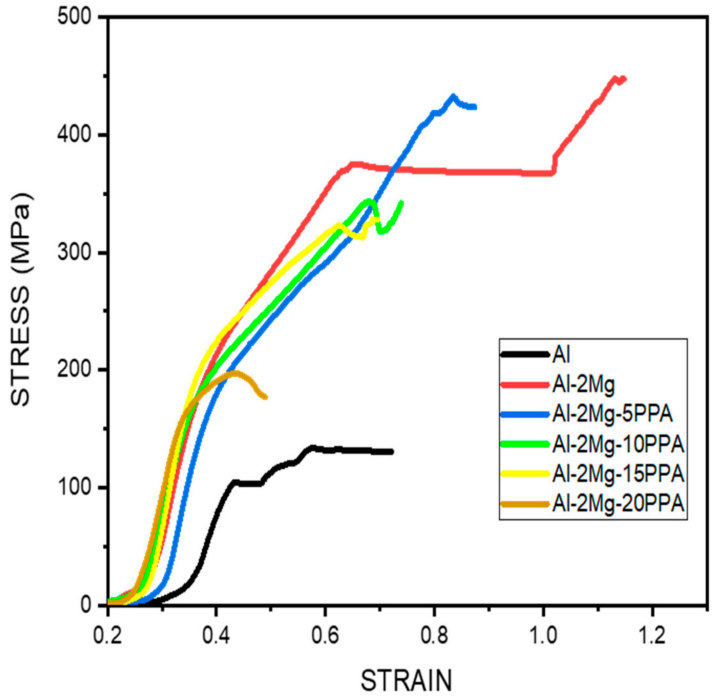


Figure 5. Stress–strain curves of Al–Mg–PPA composites under compressive load.

Table 4. Compressive strength and wear results of Al–Mg–PPA composites.

S/No.	Input Process Parameters					Responses	
	ST (°C)	'HT' (min)	SP (MPa)	Reinforcement (%wt)	HR (°C/min)	Wear Loss @ 7 N (g)	Compressive Strength (MPa)
1	430	2	12	20	50	0.003	139
2	430	4	22	15	100	0.0029	134
3	430	6	32	10	150	0.0028	203
4	430	8	42	5	200	0.0029	360
5	430	10	52	0	250	0.0031	448
6	460	2	22	10	200	0.0024	343
7	460	4	32	5	250	0.0019	432
8	460	6	42	0	50	0.0016	372
9	460	8	52	20	100	0.0015	189
10	460	10	12	15	150	0.0023	328
11	490	2	32	0	100	0.0023	354
12	490	4	42	20	150	0.0012	197
13	490	6	52	15	200	0.001	204
14	490	8	12	10	250	0.0009	295
15	490	10	22	5	50	0.0006	282
16	520	2	42	15	250	0.0013	277
17	520	4	52	10	50	0.0008	267
18	520	6	12	5	100	0.0004	310
19	520	8	22	0	150	0.0008	289
20	520	10	32	20	200	0.0014	183
21	550	2	52	5	150	0.0002	279
22	550	4	12	0	200	0.0000	213
23	550	6	22	20	250	0.0016	164
24	550	8	32	15	50	0.0009	260
25	550	10	42	10	100	0.0000	136
Al	550	4	12	100	200	0.0013	134

ST = Sintering Temperature, SP = Sintering Pressure, HT = Holding Time, HR = Heating Rate.

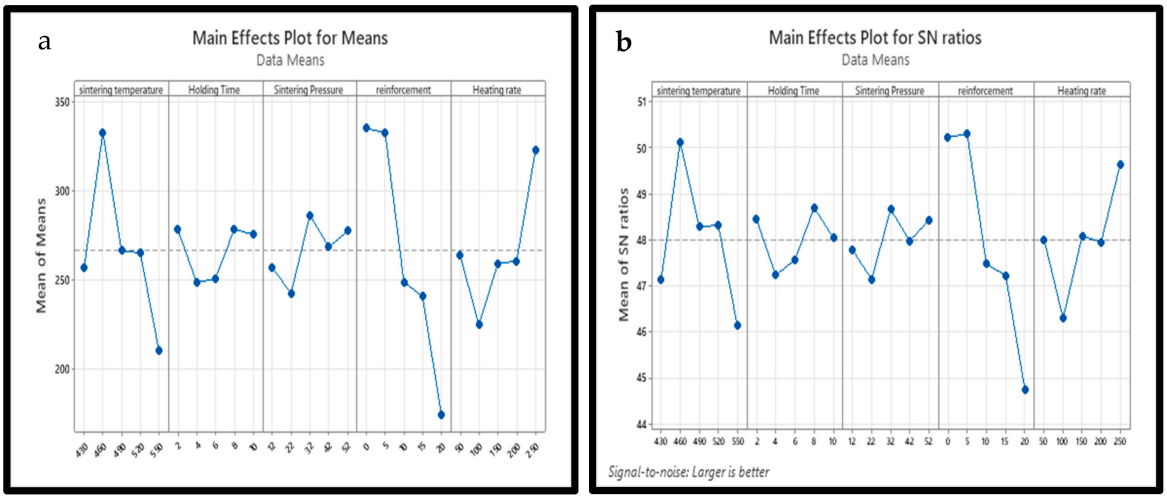


Figure 6. Main effect plots for (**a**) means and (**b**) SNRs of compressive strength.

3.3.1. Optimization of Input Parameters for Compressive Strength

The magnitudes of the effects of the input parameters on the compressive strength of Al–Mg–PPA composites are illustrated in Tables 5 and 6. As presented in both tables, the order of magnitude of each input variable from the highest to lowest includes reinforcement material (rank 1), sintering temperature (rank 2), heating rate (rank 3), sintering pressure (rank 4), and holding time (rank 5). Structural components must have high compressive strength to withstand high compression force. Similarly, the main effects plots for means and SNRs that indicate the optimal values of input parameters that maximize the compressive strength of Al–Mg–PPA composites are illustrated in Figure 6. From the figure, the optimal input parameters are the highest peaks above the dashed lines, they include a reinforcement concentration of 5 wt% PPA, a sintering temperature of 460 °C, a holding time of 8 min, a compaction pressure of 32 MPa, and a heating rate of 250 °C/min. The ANOVA result in Table 7 can be used to determine whether the impact of each input variable on the compressive strength is significant.

Table 5. Response for signal-to-noise ratios for compression strength.

Level	Sintering Temperature	Holding Time	Sintering Pressure	Reinforcement	Heating Rate
1	47.14	48.46	47.79	50.24	48.02
2	50.13	47.25	47.15	50.32	46.31
3	48.29	47.58	48.68	47.49	48.10
4	48.33	48.71	47.99	47.24	47.97
5	46.15	48.05	48.44	44.76	49.66
Delta	3.99	1.47	1.52	5.55	3.35
Rank	2	5	4	1	3

Table 6. Response for means (compressive strength).

Level	Sintering Temperature	Holding Time	Sintering Pressure	Reinforcement	Heating Rate
1	256.8	278.4	257.0	335.2	264.0
2	332.8	248.6	242.4	332.6	224.6
3	266.4	250.6	286.4	248.8	259.2
4	265.2	278.6	268.4	240.6	260.6
5	210.4	275.4	277.4	174.4	323.2
Delta	122.4	30.0	44.0	160.8	98.6
Rank	2	5	4	1	3

Table 7. ANOVA for compressive strength.

Source	DF	Adj SS	Adj MS	F-Value	*p*-Value
Regression	5	112,835	22,567.1	5.47	0.003
Temperature	1	12,864	12,864.1	3.12	0.093
Holding time	1	288	288.0	0.07	0.794
Pressure	1	2231	2231.1	0.54	0.471
Material	1	85,532	85,532.5	20.73	0.000
Heating rate	1	11,920	11,919.7	2.89	0.105
Error	19	78,378	4125.2		
Total	24	191,213			

As illustrated in Table 7, the *p*-values determine each variable's significance level. The parameters with *p*-values less than 0.05 ($p < 0.05$) are statistically significant and vice versa.

It is evident from the table that the reinforcement material has the smallest *p*-value of 0.000, which is less than the significance level of 0.05 ($p < 0.05$). This means that the influence of the reinforcement material on the compressive strength is statistically significant. The remaining input variables and their respective *p*-values in ascending order are sintering temperature ($p = 0.093$), heating rate ($p = 0.105$), sintering pressure ($p = 0.471$), and holding time ($p = 0.794$). Apart from the *p*-value for the reinforcement material, the *p*-values for the remaining parameters are larger than the significance level of 0.05 ($p > 0.05$). This means that the remaining parameters' influence on the composites' compressive strength is statistically insignificant. This is validated by the Pareto chart shown in Figure 7 using the reference line 2.093 and at a significance level of $\alpha = 0.05$. Though the influences of sintering temperature, sintering pressure, heating rate, and holding time on the compressive strength of the composite are statistically insignificant, they all contributed to the improvement in the compressive strength of the composites. For instance, as shown in Table 4 and Figure 6, the composite samples sintered at lower temperatures exhibited higher compressive strength than those sintered at higher temperatures. This agrees well with the findings of Sangmin Shin et al. [26]. Porosity in composites increases at lower sintering temperatures. One explanation for the increased compressive strength at low sintering temperatures is that porosity increases brittleness, brittleness increases with hardness, and compressive strength increases with hardness.

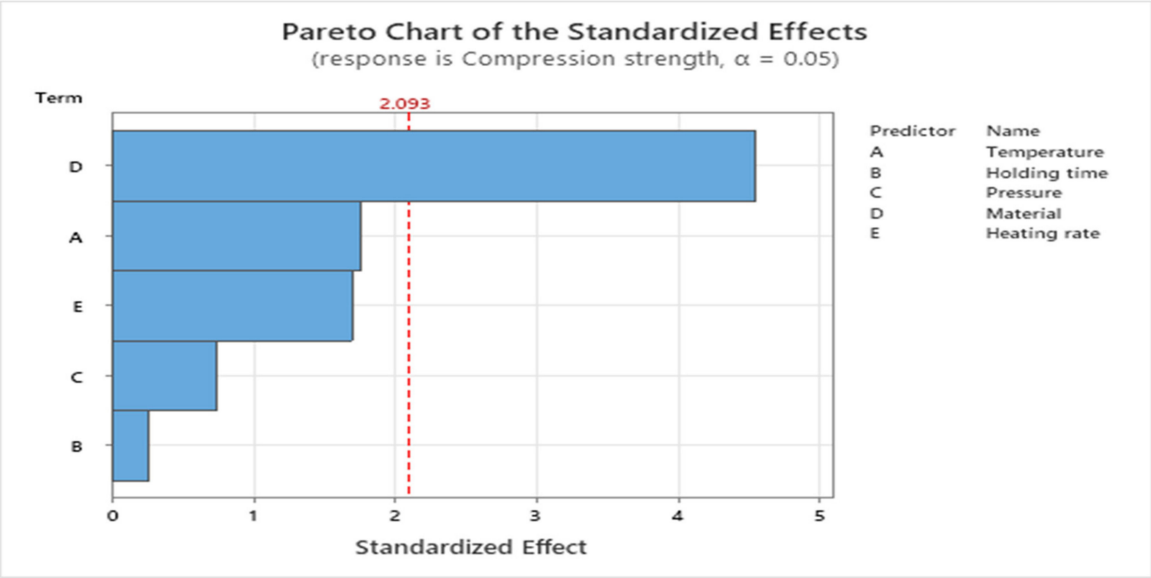


Figure 7. Pareto chart of standardized effects for wear rate.

When compared with conventional sintering, SPS offers a more effective sintering process since the sintering pressure and temperature are applied simultaneously. Increasing the compaction pressure of composites in powder metallurgy causes the composite powder particles to flow more plastically, enhancing mechanical properties [27]. It is evident from Figure 6 that a sintering pressure of 32 MPa was optimal to avoid excessive deformation, which can adversely affect the compressive strength of the Al–Mg–PPA composites. From Table 4, it is observed that the sintering pressure has a decreasing effect on compressive strength as the concentration of PPA reinforcement rises. This can be explained by the fact that as the PPA's percentage weight fraction rises, the wettability between the Al matrix and the reinforcement decreases. It can be argued that wettability between material phases determines the efficacy of the compaction pressure, and wettability also influences strong interfacial bonds. Additionally, because of the poor plastic flow of ceramic powder particles, the increased volume fraction of PPA reinforcement reduces the compressibility of the composite powder particles, thereby impairing compressive strength. Furthermore, the heating rate of a spark plasma sintering machine can be as high as 1000 °C/min, so it

takes a shorter time to attain the desired sintering temperature and a short holding time to prevent grain growth. This explains why a higher heating rate requires a short holding time, as depicted in Figure 6.

3.3.2. Effect of Reinforcement Characteristics on Compressive Strength

The impact of the weight fractions of PPA reinforcement on the compressive strength of Al–Mg–PPA composites has been investigated. Several reasons can be attributed to the enhanced compressive strength of the composites. It is evident from Table 5 that the compressive strength of the composites improved due to the addition of PPA reinforcement. Significant improvement was observed for composites reinforced with 5 wt% PPA. However, at high-volume PPA reinforcement, the composites' compressive strength diminished. Owing to the density differential between the ceramic reinforcement and the matrix metal, adding ceramic reinforcement to metal matrices frequently causes particle clustering and poor surface adhesion. This may be why the compressive strength dropped at a higher PPA reinforcement volume. Strong interfacial bonding depends on the degree of wettability between material phases. In this study, 2 wt% Mg powder was added to the Al matrix and PPA powder mixture to improve the wettability [28]. As earlier stated, the strong interfacial bond between the aluminum matrix and the PPA reinforcement is responsible for the enhanced compressive strength of some of the sintered AMC.

It can be deduced from Figures 2 and 3 that the PPA and Mg powders were evenly dispersed within the Al matrix. The homogeneity of the Al and PPA powder mixture is required for improved compressive strength of the composites. Particle agglomeration impairs compressive strength by increasing pores, which may result in micro-cracks and weak interfacial bonding. The uniform dispersion of the PPA powder particles within the aluminum matrix inhibits the clumping of particles; however, at high-volume PPA reinforcement, particle agglomeration may become inevitable. Furthermore, the consistent decline in the compressive strength of the composites reinforced with 20 wt% PPA may be due to the weak phase of the PPA reinforcement, which impairs its load-bearing capacity. Therefore, compressive strength decreases as the concentration of the soft or weak grains increases in the composites.

More so, the compressive strength of Al–Mg–PPA can further be improved by grain refinement or grain size reduction. The argument for this is that fine grains are prone to misalignment, which makes it more difficult for a dislocation to spread to neighboring grains. Plastic deformation is difficult because of the larger dislocation density resulting from smaller grains, which act as a barrier to dislocation motion. As expressed in Equations (7)–(9), a decrease in the reinforcements' and matrix's particle size improves the composites' compressive strength. This is because dislocation motion involving fine grains requires more energy than coarse grains. Compared to soft grains, hard grains make dislocation motion even more difficult [24,29–31].

$$\sigma_y = \sigma_0 + kd^{-1/2} \tag{7}$$

$$\tau = \frac{Gb}{\lambda} \tag{8}$$

$$\lambda = \frac{4(1-f)r}{3f} \tag{9}$$

where σ_y is the flow stress, σ_0 and k are constant, d is the grain size, τ is the shear stress required for a dislocation motion through the secondary phase, G is the shear modulus of rigidity, b is the Bergers vector, λ is the distance between reinforcement particles, f is the volume fraction of the reinforcement particles, and r is the radius of the particles, assuming they are spherical.

The Hall–Petch equation expressed in Equation (7) states that when the particle size of composites reduces, the stress necessary to induce dislocation motion rises, increasing compressive strength. Equations (8) and (9) show that the distance between particles

decreases as their radius decreases, creating more barriers to impede dislocation motion and the formation of grain boundaries. Particle agglomeration, however, becomes unavoidable at high reinforcement volume fractions, reducing the composites' capacity to withstand compression [31]. This elucidates why the compressive strength of the fabricated Al–Mg–PPA composites dropped as the volume fraction of PPA increased.

3.4. Fracture Surface Morphology

The fracture surfaces of the Al–Mg–PPA composites are shown in Figure 8a–f. Tear ridges, shear steps, micro-voids, and cleavages indicate a ductile-brittle fracture. Brittleness increases as ductility decreases with increasing porosity. The PPA reinforcement is porous, and when the concentration of the PPA rises, an increasingly brittle phase develops in the composites [32,33]. Tear ridges, a few micro-voids, and cleavages suggestive of ductile-brittle fracture are the primary features of Figure 8a. The presence of tear ridges in Figure 8a shows that significant plastic deformation occurred before fracture. A combination of tear ridges, shear tears, micro-voids, and cleavages can be seen on the fracture surfaces in Figure 8c,e,f. It is evident from the figures that the composite samples took in some energy before breaking. Brittleness increases as the PPA concentration rises to 15 wt% and 20 wt% in the composites displayed in Figure 8d,b.

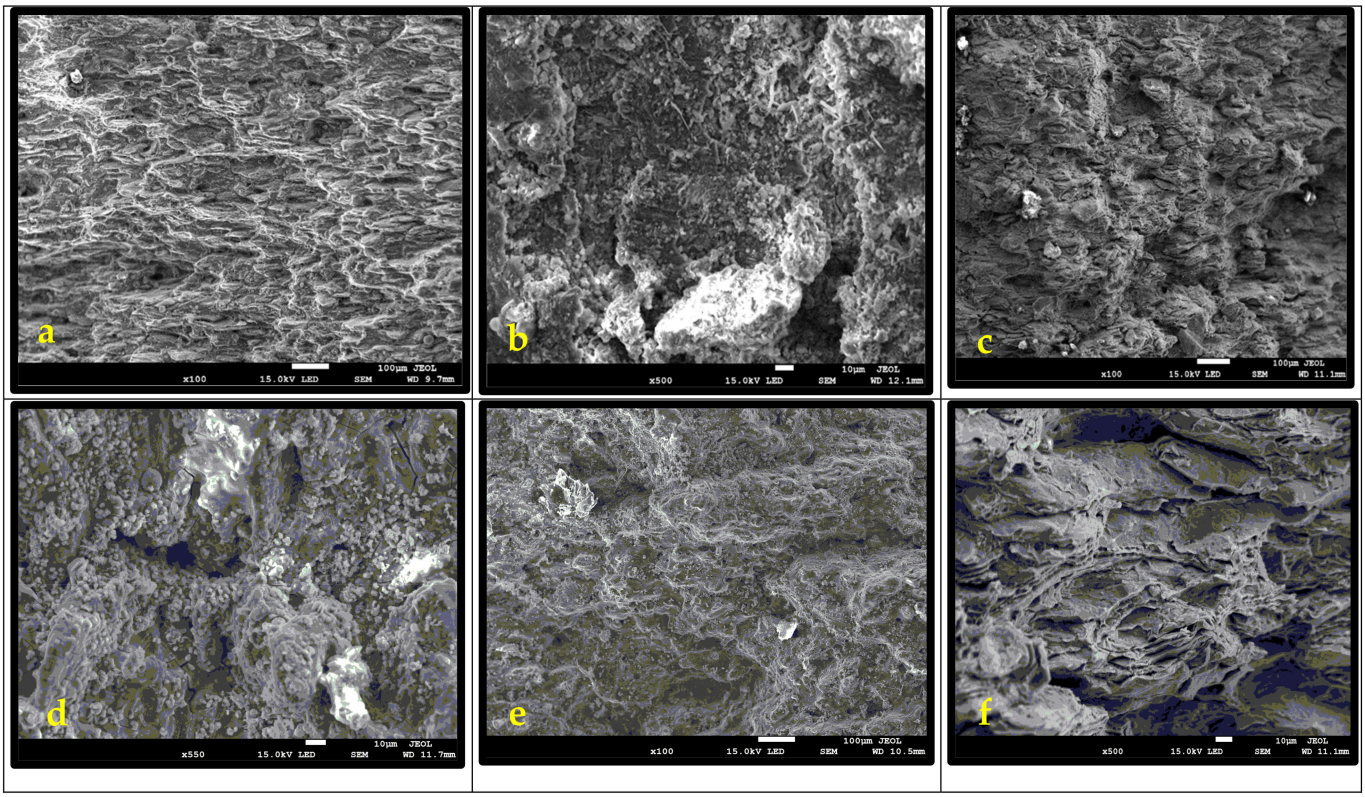


Figure 8. SEM fracture surfaces of Al–Mg–PPA composites (**a**) Al–2Mg–5PPA, (**b**) Al–2Mg–20PPA, (**c**) Al–2Mg, (**d**) Al–2Mg–15PPA, (**e**) Al–2Mg–10PPA, and (**f**) Al–2Mg.

3.5. Wear Characteristics of Al–Mg–PPA Composites

As presented in Table 4 and Figure 9, the wear resistance of the sintered Al–Mg–PPA composites was evaluated in terms of mass loss (difference in mass of the sample before and after the wear test). From Figures 9–14), B0 to B5 represent the samples' material compositions, which include B0 = Al, B1 = Al–2Mg, B2 = Al–2Mg–5PPA, B3 = Al–2Mg–10PPA, B4 = Al–2Mg–15PPA, and B5 = Al–2Mg–20PPA. Comparing Figure 9a with Figure 9b reveals that composites sintered at higher temperatures display higher wear resistance than those sintered at lower temperatures. Higher densification and strong interfacial bonds

are achieved at higher temperatures. Therefore, the wear rate of the sintered Al/Mg/PPA composites is influenced by the density, interfacial bonding, and metallographic defects such as porosity and micro-cracks. It can be deduced from Figure 9b that the wear resistance of the composite samples improved considerably due to the addition of PPA reinforcement and Mg wetting agent. As seen from Figure 9b, the masses of samples B1 and B3 remained the same after a sliding distance of 5 m and under an applied load of 7 N, an indication of high wear resistance. However, at 20 wt% PPA reinforcement, the wear resistance of the composites declined. This can be attributed to several factors, such as the weak phase of the PPA reinforcement, increased porosity, and decreased wettability between the Al and PPA phases. When compared with synthetic reinforcement such as SiC, the PPA is a weaker phase. At high-volume PPA reinforcement, the percentage fraction of the weak phase in the composites increases, resulting in a decline in the wear resistance. According to Figure 10, the optimal PPA reinforcement volume for optimum wear resistance is 5 wt% PPA.

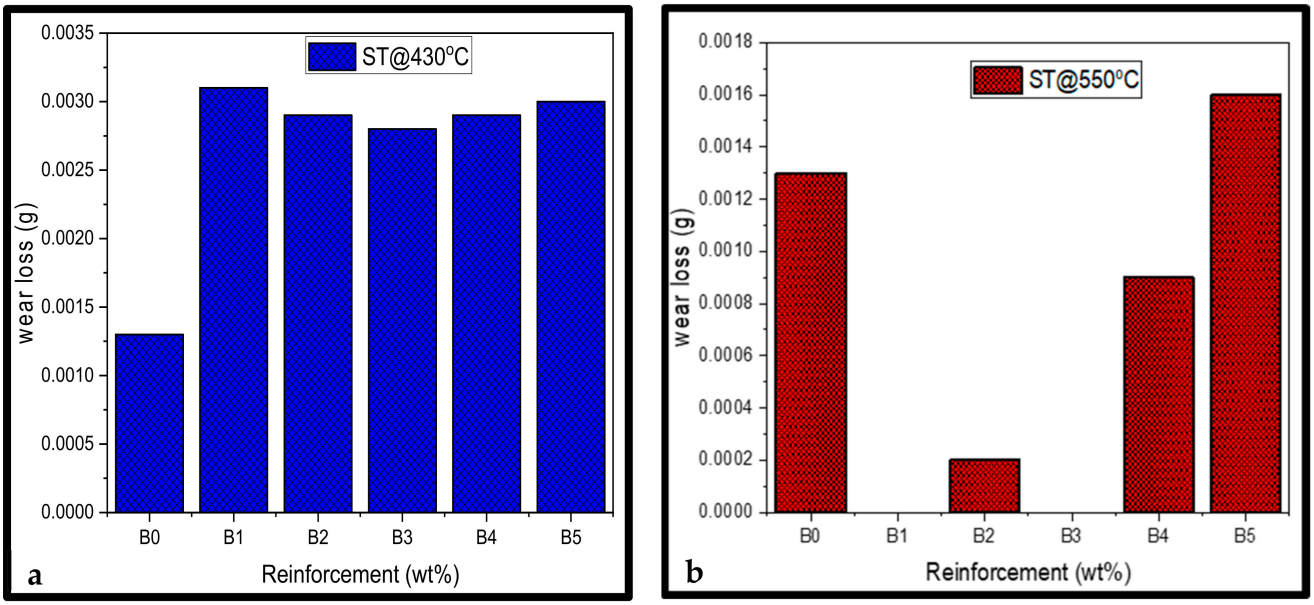


Figure 9. Effects of input parameters on the wear rates of Al–Mg–PPA composites (**a**) samples sintered at 430° (**b**) samples sintered at 550°.

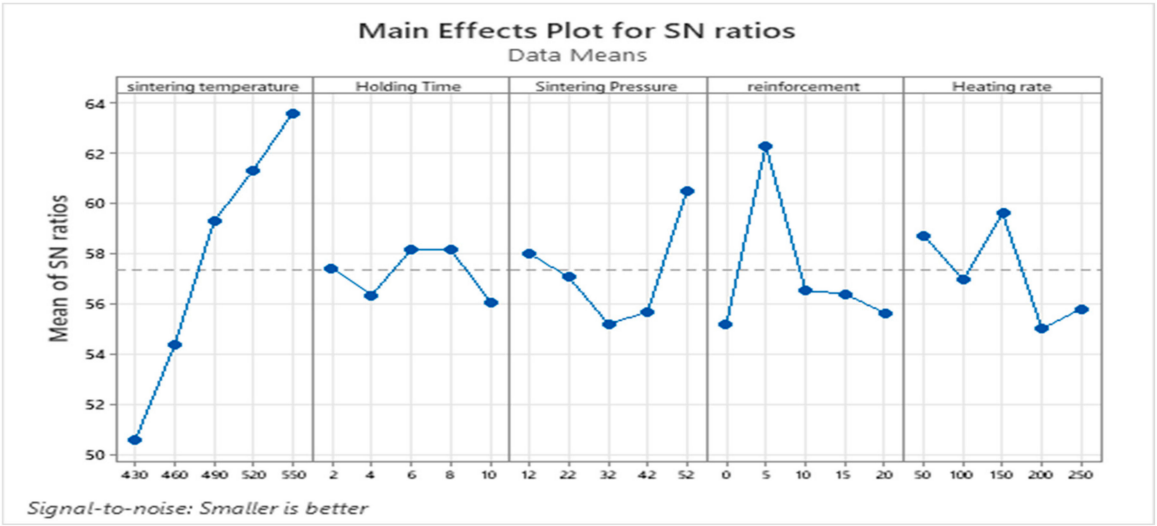


Figure 10. Main effects plots for SNRs of wear loss.

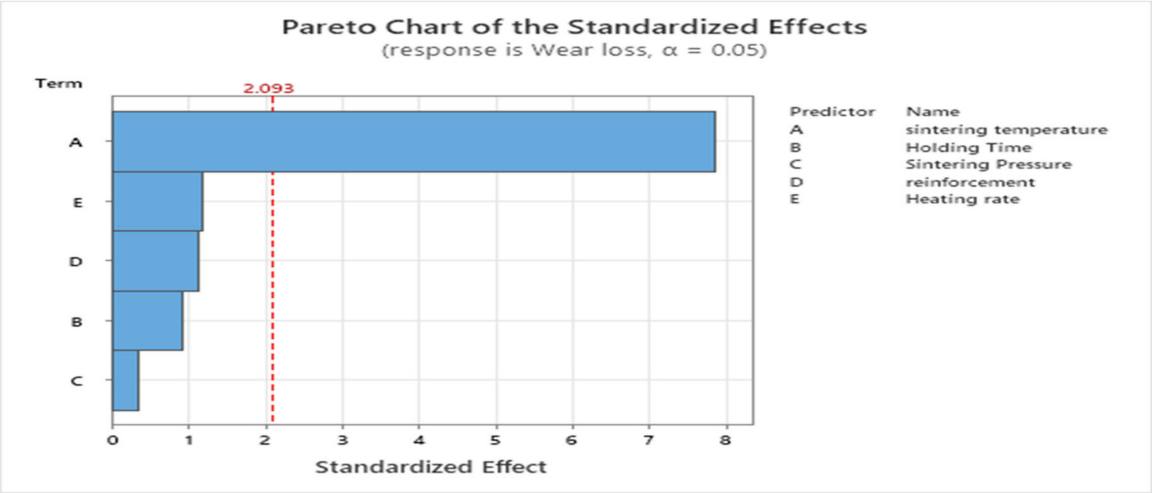


Figure 11. Pareto chart of standardized effects for wear loss.

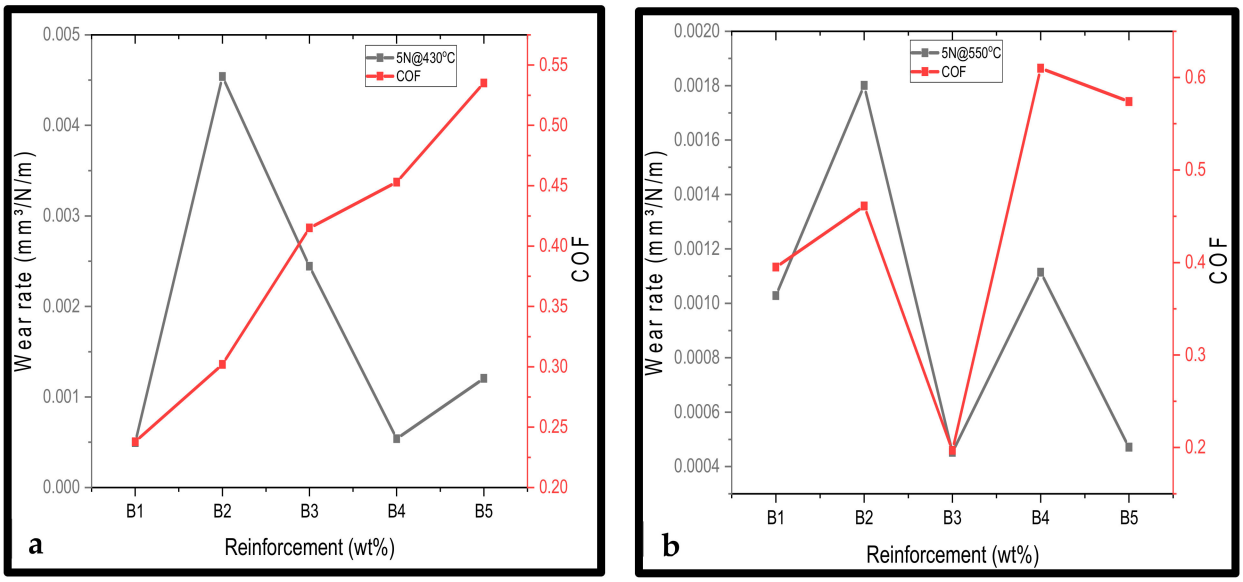


Figure 12. Relationship between wear rate and COF of Al–Mg–PPA samples sintered at different temperatures (**a**) sintered at 430° (**b**) sintered at 550°.

The magnitudes of the effects of the input parameters on the wear rates of the Al–Mg–PPA composites are illustrated in Tables 8 and 9. Both tables indicate that the sintering temperature has the strongest impact on the wear rate (rank 1), secondly by the reinforcement material (rank 2), and thirdly by the sintering pressure. However, there is a disparity between Tables 8 and 9 regarding which of the parameters between holding time and the heating rate has the weakest effect on the wear loss of the composites. From Figure 10, the optimal values of input parameters representing the highest peaks above the dashed lines can easily be identified. They include a sintering temperature of 550 °C, a holding time of 6 or 8 min, a sintering pressure of 52 MPa, a reinforcement weight fraction of 5 wt% PPA, and a heating rate of 150 °C. Therefore, the wear rate of the AMC can be reduced by optimizing the input variables.

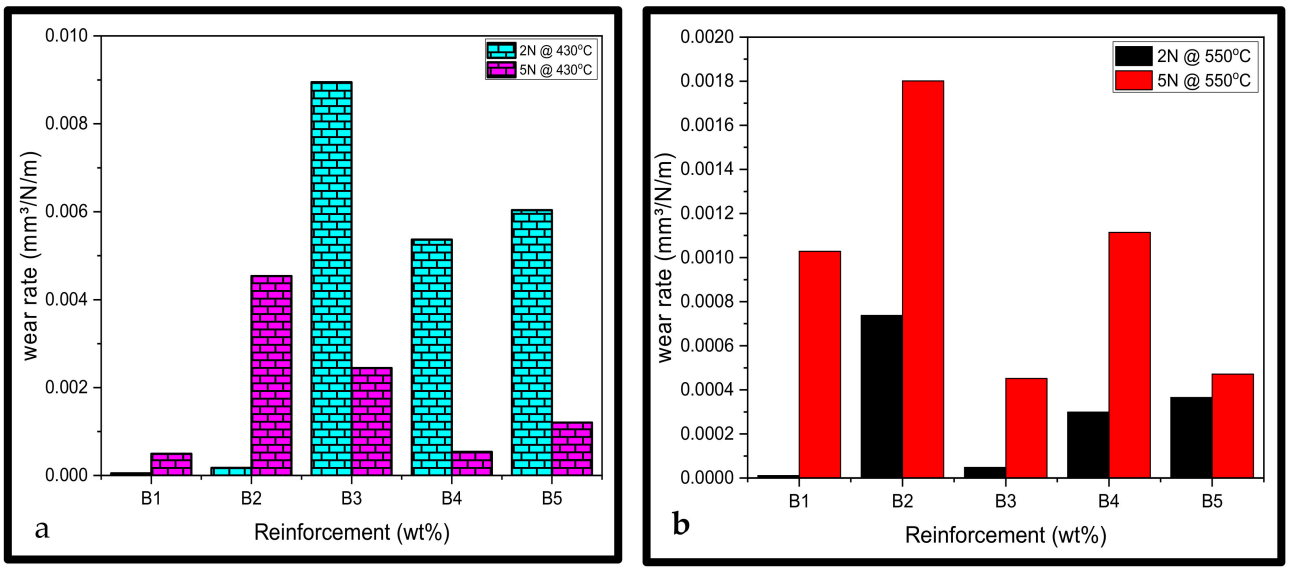


Figure 13. Effect of applied load on the wear rate of Al–Mg–PPA samples sintered at different temperatures (**a**) sintered at 430° (**b**) sintered at 550°.

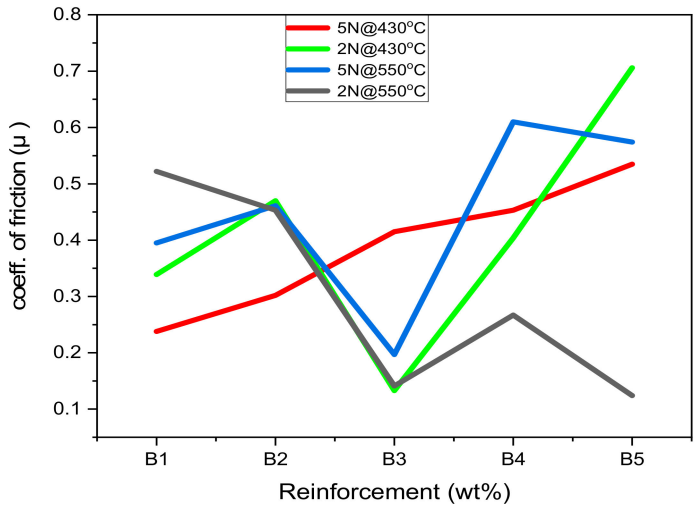


Figure 14. Effects of wear load on the COFs of Al–Mg–PPA composites.

Table 8. Response table for signal-to-noise ratios (wear rate).

Level	Sintering Temperature	Holding Time	Sintering Pressure	Reinforcement	Heating Rate
1	50.64	57.46	58.02	55.20	58.73
2	54.40	56.38	57.09	62.31	56.99
3	59.31	58.17	55.25	56.58	59.63
4	61.33	58.20	55.70	56.43	55.06
5	63.60	56.11	60.51	55.67	55.83
Delta	12.97	2.09	5.27	7.11	4.57
Rank	1	5	3	2	4

Table 9. Response for means (wear rate).

Level	Sintering Temperature	Holding Time	Sintering Pressure	Reinforcement	Heating Rate
1	0.002940	0.001840	0.001320	0.001560	0.001380
2	0.001940	0.001360	0.001660	0.001200	0.001420
3	0.001200	0.001480	0.001860	0.001380	0.001460
4	0.000940	0.001400	0.001400	0.001680	0.001540
5	0.000540	0.001480	0.001320	0.001740	0.001760
Delta	0.002400	0.000480	0.000540	0.000540	0.000380
Rank	1	4	3	2	5

The ANOVA results in Table 10 can be used to determine each input parameters' influence on the wear loss and their significant levels.

Table 10. ANOVA for wear loss.

Source	DF	Adj SS	Adj MS	F-Value	*p*-Value
Regression	5	0.000018	0.000004	13.12	0.000
Temperature	1	0.000017	0.000017	61.92	0.000
Holding Time	1	0.000000	0.000000	0.85	0.368
Pressure	1	0.000000	0.000000	0.12	0.728
Reinforcement	1	0.000000	0.000000	1.30	0.269
Heating rate	1	0.000000	0.000000	1.43	0.247
Error	19	0.000005	0.000000		
Total	24	0.000023			

From the ANOVA results in Table 10, the sintering temperature is the only input factor whose impact on the wear loss is statistically significant ($p < 0.05$). This is also confirmed by the Pareto chart illustrated in Figure 11, based on the reference line 2.093 and at a significance level of $\alpha = 0.05$. Besides the sintering temperature, the remaining input variables, such as the reinforcement material, sintering pressure, heating rate, and holding time, also influenced the wear properties of the Al–Mg–PPA composites. Like the PPA reinforcement, several studies have reported the significant role reinforcement materials play in reducing the wear rates of MMCs. For instance, reinforcement materials such as graphite and fullerene have lubricating properties and, as a result, considerably reduce the wear rates of AMCs [6]. Other reinforcement materials such as TiC, B_4C, and SiC increased the wear resistances of AMCs by enhancing the hardness property [7,8].

There is a correlation between the COF and the wear rate of the sintered composites, as illustrated in Figure 12. It can be seen from Figure 12a that the COF rises as the composites' wear rates increase. In contrast to most studies, the COF continues to increase as the wear rate drops. More so, it can be seen from Figure 12b that the COF rises with increasing wear rate and decreases with decreasing wear rate. At higher sintering temperatures, low porosity and strong interfacial bonds are attained. Therefore, it can be deduced from Figure 12b that the composites sintered at 550 °C had a higher densification and little to no microstructural defects than those sintered at 430 °C. For such composites sintered at elevated temperatures, the COF decreases as the wear rate decreases and vice versa. This result is consistent with the findings of Raghav et al. [14] and Ayodele et al. [34].

Figures 13 and 14 show the effect of wear load on the wear rate and COF of Al–Mg–PPA composites, respectively. It is evident from Figure 13a that apart from the B2 (Al–2Mg–5PPA) composite sample, the increase in wear load from 2 N to 5 N did not increase the wear rate. From Figure 13b, the wear rates of all the composite samples increased as the wear load increased from 2 N to 5 N. While the outcome of Figure 13b is consistent with most findings, the outcome of Figure 13a is the converse [14,34]. This is because an increase in wear load increases the plastic strain, consequently increasing the wear rate.

Microstructural conditions, including increased porosity and other microstructural flaws, are responsible for the results seen in Figure 13a. Likewise, Figure 14 makes it clear

that the COF did not rise in proportion to the increase in wear load from 2 N to 5 N. The sintered Al–Mg–PPA composites were shown to readily oxidize to provide a thin oxide layer that serves as a lubricant [14]. AMC continuously re-oxidizes on the surfaces to create an oxide layer that is thin and protective against wear. This may be the cause of some sintered Al–Mg–PPA composites' decreased wear rates and COFs, despite the increase in wear loads.

Wear Surface Morphology

The SEM micrographs of the worn surfaces of Al–Mg–PPA composites under a wearing load of 7 N are shown in Figure 15. As seen from the figure, the worn surfaces are characterized by scratches, ripples, and deep grooves, which is typical of abrasive wear [11]. It is also obvious that the wear tracks resulted from plastic deformation, grain cutting, and pull-out, characteristic of a softer base (sintered AMC) and weak interfacial boundaries. The abrasive wear mechanism confirms that the tribometer pin bearing the wear load is harder than the sintered Al–Mg–PPA composites. Some factors influencing abrasive wear include the applied load, sliding velocity, sliding distance, temperature, and the base material characteristics.

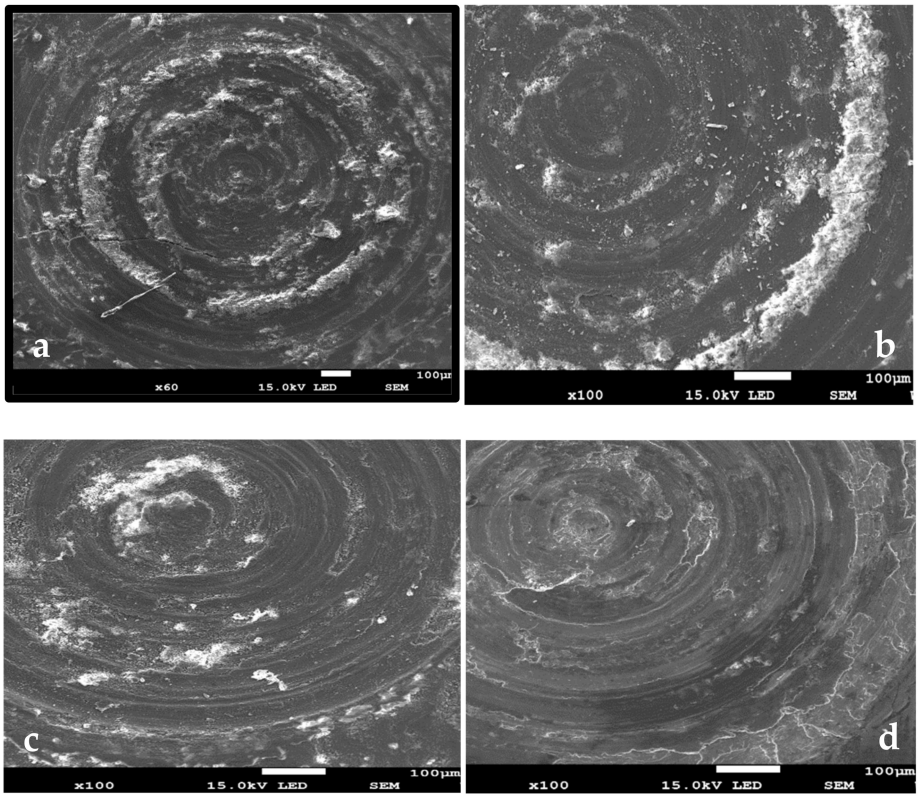


Figure 15. Worn out surfaces of Al–Mg–PPA composites (**a**) Al–2Mg–20PPA, (**b**) Al–2Mg–15PPA, (**c**) Al–2Mg–5PPA, and (**d**) Al–2Mg.

4. Conclusions

Al–Mg–PPA composites were successfully fabricated in this research. Spark plasma sintering was used to sinter composites, and favorable mechanical properties, surface morphology, and wear characteristics were obtained. The following conclusions can be drawn from this research:

i. The optical and SEM micrographs revealed that the composites' microstructural features are well enhanced, with little to no microstructural defects.

ii. The Al–Mg–PPA composites' enhanced compressive and wear properties can be attributed to the PPA reinforcement, the Mg powder as a wetting agent, the high efficiency of ball milling, and the SPS technology.
iii. The optimal input variables for compressive strength are a reinforcement concentration of 5 wt% PPA, a sintering temperature of 460 °C, a holding time of 8 min, a compaction pressure of 32 MPa, and a heating rate of 250 °C.
iv. The optimal input variables for wear loss include a sintering temperature of 550 °C, a holding time of 6 or 8 min, a sintering pressure of 52 MPa, a reinforcement weight fraction of 5 wt% PPA, and a heating rate of 150 °C.

Author Contributions: Conceptualizing and designing experiments—O.O.E., F.K.T., P.A.O. and K.G.; investigation and software—O.O.E.; analysis and optimization—O.O.E., F.K.T., P.A.O. and K.G.; writing original draft—O.O.E.; review, editing, and supervision—F.K.T., P.A.O. and K.G. All authors have read and agreed to the published version of the manuscript.

Funding: This research received no external funding.

Data Availability Statement: Data are available upon request.

Acknowledgments: We acknowledge the assistance provided by the Metallurgy and Mechanical laboratory staff of the University of Johannesburg.

Conflicts of Interest: The authors declare that they have no known competing financial interests or personal relationships that could have appeared to influence the research reported in this paper.

References

1. Liu, Y.; Ma, Y.; Liu, W.; Huang, Y.; Wu, L.; Wang, T.; Liu, C.; Yang, L. The mechanical properties and formation mechanism of Al/Mg composite interface prepared by spark plasma sintering under different sintering pressures. *Vacuum* **2020**, *176*, 109300. [CrossRef]
2. Bodunrin, M.O.; Alaneme, K.K.; Chown, L.H. Aluminium matrix hybrid composites: A review of reinforcement philosophies; Mechanical, corrosion and tribological characteristics. *J. Mater. Res. Technol.* **2015**, *4*, 434–445. [CrossRef]
3. Venkatesh, V.S.S.; Deoghare, A.B. Modelling and Optimisation of Wear Parameters for Spark Plasma Sintered Al– SiC–Kaoline Hybrid Composite. *Adv. Mater. Process. Technol.* **2021**, *8*, 1286–1304. [CrossRef]
4. Sharma, A.K.; Bhandari, R.; Aherwar, A.; Rimašauskiene, R.; Pinca-Bretotean, C. A study of advancement in application opportunities of aluminum metal matrix composites. *Mater. Today Proc.* **2020**, *26*, 2419–2424. [CrossRef]
5. Samal, P.; Vundavilli, P.R.; Meher, A.; Mahapatra, M.M. Recent progress in aluminum metal matrix composites: A review on processing, mechanical and wear properties. *J. Manuf. Process.* **2020**, *59*, 131–152. [CrossRef]
6. Maclin John Vasanth, K.; Lokendar Ram, P.S.; Pon Anand, V.; Prabu, M.; Rahul, S. Experimental investigation of mechanical and tribological properties of Aluminium metal matrix composites fabricated by powder metallurgy route—A review. *Mater. Today Proc.* **2020**, *33*, 1058–1072. [CrossRef]
7. Irhayyim, S.S.; Hammood, H.S.; Mahdi, A.D. Mechanical and wear properties of hybrid aluminum matrix composite reinforced with graphite and nano MgO particles prepared by powder metallurgy technique. *AIMS Mater. Sci.* **2020**, *7*, 103–115. [CrossRef]
8. Pradeep Devaneyan, S.; Ganesh, R.; Senthilvelan, T. On the Mechanical Properties of Hybrid Aluminium 7075 Matrix Composite Material Reinforced with SiC and TiC Produced by Powder Metallurgy Method. *Indian J. Mater. Sci.* **2017**, *2017*, 3067257. [CrossRef]
9. Mavhungu, S.T.; Akinlabi, E.T.; Onitiri, M.A.; Varachia, F.M. Aluminum Matrix Composites for Industrial Use: Advances and Trends. *Procedia Manuf.* **2017**, *7*, 178–182. [CrossRef]
10. Singh, L.; Singh, B.; Saxena, K.K. Manufacturing techniques for metal matrix composites (MMC): An overview. *Adv. Mater. Process. Technol.* **2020**, *6*, 224–240. [CrossRef]
11. Shaikh, M.B.N.; Aziz, T.; Arif, S.; Ansari, A.H.; Karagiannidis, P.G.; Uddin, M. Effect of sintering techniques on microstructural, mechanical and tribological properties of Al-SiC composites. *Surf. Interfaces* **2020**, *20*, 100598. [CrossRef]
12. Pramanik, A. Effects of reinforcement on wear resistance of aluminum matrix composites. *Trans. Nonferrous Met. Soc. China* **2016**, *26*, 348–358. [CrossRef]
13. Mohammad Sharifi, E.; Karimzadeh, F.; Enayati, M.H. Fabrication and evaluation of mechanical and tribological properties of boron carbide reinforced aluminum matrix nanocomposites. *Mater. Des.* **2011**, *32*, 3263–3271. [CrossRef]
14. Raghav, G.R.; Janardhanan, S.; Sajith, E.; Chandran, V.; Sruthi, V. Mechanical and tribological performance of Al-Fe-SiC-Zr hybrid composites produced through powder metallurgy process. *Mater. Res. Express* **2021**, *8*, 016533. [CrossRef]
15. Aynalem, G.F. Processing Methods and Mechanical Properties of Aluminium Matrix Composites. *Adv. Mater. Sci. Eng.* **2020**, *2020*, 3765791. [CrossRef]

16. Sharma, S.K.; Saxena, K.K.; Salem, K.H.; Mohammed, K.A.; Singh, R.; Prakash, C. Effects of various fabrication techniques on the mechanical characteristics of metal matrix composites: A review. *Adv. Mater. Process. Technol.* **2024**, *10*, 277–294. [CrossRef]
17. Sarmah, P.; Gupta, K. Recent Advancements in Fabrication of Metal Matrix Composites: A Systematic Review. *Materials* **2024**, *17*, 4635. [CrossRef]
18. Trapp, J.; Semenov, A.; Eberhardt, O.; Nöthe, M.; Wallmersperger, T.; Kieback, B. Fundamental principles of spark plasma sintering of metals: Part II—About the existence or non-existence of the 'spark plasma effect. *Powder Metall.* **2020**, *63*, 312–328. [CrossRef]
19. Manohar, G.; Pandey, K.M.; Maity, S.R. Effect of spark plasma sintering on microstructure and mechanical properties of AA7075/B4C/ZrC hybrid nanocomposite fabricated by powder metallurgy techniques. *Mater. Chem. Phys.* **2022**, *282*, 126000. [CrossRef]
20. Bharathi, P.; Kumar, T.S. Mechanical Characteristics and Wear Behaviour of Al/SiC and Al/SiC/B4C Hybrid Metal Matrix Composites Fabricated Through Powder Metallurgy Route. *Silicon* **2023**, *15*, 4259–4275. [CrossRef]
21. Arunkumar, S.; Kumar, A.S. Studies on Egg Shell and SiC Reinforced Hybrid Metal Matrix Composite for Tribological Applications. *Silicon* **2022**, *14*, 1959–1967. [CrossRef]
22. Ponhan, K.; Tassenberg, K.; Weston, D.; Nicholls, K.G.M.; Thornton, R. Effect of SiC nanoparticle content and milling time on the microstructural characteristics and properties of Mg-SiC nanocomposites synthesized with powder metallurgy incorporating high-energy ball milling. *Ceram. Int.* **2020**, *46*, 26956–26969. [CrossRef]
23. Seyed Pourmand, N.; Asgharzadeh, H. Aluminum Matrix Composites Reinforced with Graphene: A Review on Production, Microstructure, and Properties. *Crit. Rev. Solid State Mater. Sci.* **2020**, *45*, 289–337. [CrossRef]
24. Anand Sekhar, R.; Rakesh Pillai, R.; Mubarak Ali, M.; Shyam Kumar, C. Enhanced mechanical and wear properties of aluminium-based composites reinforced with a unique blend of granite particles and boron carbide for sustainable material recycling. *J. Alloys Compd.* **2023**, *963*, 171165. [CrossRef]
25. Akbarpour, M.R. Microstructure, Densification, and Compressive Properties of Al-CNT Metal Matrix Composites Fabricated by Flake Powder Metallurgy and Conventional Sintering Process. *Adv. Ceram. Prog.* **2022**, *8*, 27–33.
26. Shin, S.; Cho, S.; Lee, D.; Kim, Y.; Lee, S.-B.; Lee, S.-K.; Jo, I. Microstructural Evolution and Strengthening Mechanism of SiC/Al Composites Fabricated by a Liquid-Pressing Process and Heat Treatment. *Materials* **2019**, *12*, 3374. [CrossRef]
27. Pichi Reddy, S.; Ramana, B.; Chennakesava Reddy, A. Sintering characteristics of Al-Pb/fly-ash metal matrix composites. *Trans. Indian Inst. Met.* **2013**, *66*, 87–95. [CrossRef]
28. Tosun, G.; Kurt, M. The porosity, microstructure, and hardness of Al-Mg composites reinforced with micro particle SiC/Al2O3 produced using powder metallurgy. *Compos. Part B Eng.* **2019**, *174*, 106965. [CrossRef]
29. Shorowordi, K.M.; Laoui, T.; Haseeb, A.S.M.A.; Celis, J.P.; Froyen, L. Microstructure and interface characteristics of B4C, SiC and Al2O3 reinforced Al matrix composites: A comparative study. *J. Mater. Process. Technol.* **2003**, *142*, 738–743. [CrossRef]
30. Rahimian, M.; Ehsani, N.; Parvin, N.; Baharvandi, H. The effect of particle size, sintering temperature and sintering time on the properties of Al-Al2O3 composites, made by powder metallurgy. *J. Mater. Process. Technol.* **2009**, *209*, 5387–5393. [CrossRef]
31. Sadiq, G.S.; Abd, A.N.; Ameen, A.A. Microstructure Analysis and Compression Strength Investigation of the Copper Reinforced with Nano & Micro Particles of Alumina. *Int. J. Appl. Eng. Res.* **2018**, *13*, 5926–5934.
32. Brillon, A.; Garcia, J.; Riallant, F.; Garnier, C.; Joulain, A.; Lu, Y.; Silvain, J.F. Characterization of Al/B4C composite materials fabricated by powder metallurgy process technique for nuclear applications. *J. Nucl. Mater.* **2022**, *565*, 153724. [CrossRef]
33. Venkatesh, V.S.S.; Deoghare, A.B. Effect of Sintering Mechanisms on the Mechanical Behaviour of SiC and Kaoline Reinforced Hybrid Aluminium Metal Matrix Composite Fabricated through Powder Metallurgy Technique. *Silicon* **2022**, *14*, 5481–5493. [CrossRef]
34. Ayodele, O.O.; Babalola, B.J.; Olubambi, P.A. Characterization, nanomechanical, and wear attributes of sintered Al–TiB2 composites. *J. Mater. Res. Technol.* **2023**, *24*, 4153–4167. [CrossRef]

Disclaimer/Publisher's Note: The statements, opinions and data contained in all publications are solely those of the individual author(s) and contributor(s) and not of MDPI and/or the editor(s). MDPI and/or the editor(s) disclaim responsibility for any injury to people or property resulting from any ideas, methods, instructions or products referred to in the content.